# Human ACE2 Peptide Attached Plasmonic-Magnetic Heterostructure for Magnetic Separation, SERS Identification, and Inhibition of Different Variants of SARS-CoV-2 Infections

**Avijit Pramanik[1], Justin Mayer[2], Sudarson Sekhar Sinha[1], Poonam C. Sharma [3], Shamily Patibandla[1], Ye Gao[1], John T. Bates [3], Michael A. Bierdeman[3], Ritesh Tandon[3], Ram Seshadri [2] and Paresh Chandra Ray[1] ***

[1]Department of Chemistry and Biochemistry, Jackson State University, Jackson, MS, 39217, USA; E-mail: paresh.c.ray@jsums.edu; Fax: +16019793674

[2]Materials Department, University of California, Santa Barbara, California 93106-5121, United States

[3]Department of Microbiology and Immunology, University of Mississippi Medical Center, Jackson, MS, 39216, USA

---

**ABSTRACT:** The emergence of Alpha, Beta, Gamma, Delta, and Omicron variants of the severe acute respiratory syndrome coronavirus 2 (SARS-CoV-2) is responsible for several millions of deaths till now. Due to the huge amount of vaccine escape mutation in the spike (S) protein for different variants, the design of new material for combating SARS-CoV-2 is very important for our society. Herein, we report for the design of human Angiotensin Converting Enzyme 2 (ACE2) peptide conjugated plasmonic-magnetic hetero structure, which has capability for magnetic separation, identification via surface enhanced Raman spectroscopy (SERS) and inhibition of different variant SARS-CoV-2 infections. In this work, plasmonic-magnetic heterostructure were developed using initial synthesis of polyethyleneimine (PEI) coated $Fe_3O_4$ based magnetic nanoparticles and then gold nanoparticles (GNPs) were grown onto the surface of magnetic nanoparticles by the citrate reduction of $Au^{3+}$. Experimental binding data between ACE2 conjugated plasmonic-magnetic heterostructure and spike- receptor-binding domain (RBD) shows omicron has maximum binding ability and it follows Alpha < Beta < Gamma < Delta < Omicron. Our finding shows that, due to the high magnetic moment (specific magnetization 40 emu/g), bio-conjugated hetero structures are capable of effective magnetic separation of pseudotyped SARS-CoV-2 bearing the Delta variant spike from infected artificial nasal mucus fluid sample using a simple bar magnet. Experimental data shows that due to the formation of huge "hot spots" in the presence of SARS-CoV-2, Raman intensity for 4-aminothiolphenol (4-ATP) Raman reporter enhanced abruptly, which has been used for the identification of separated virus. Theoretical calculation using finite-difference time-domain (FDTD) simulation indicates due to the "hot spots" formation six orders of magnitude Raman enhancement can be observed. Concentration dependent inhibition efficiency investigation using HEK293T-human cell line indicates that ACE2 peptide conjugated plasmonic-magnetic hetero structures has capability for complete inhibition of Delta variants and original SARS-CoV-2 pseudo virions entry into host cells.

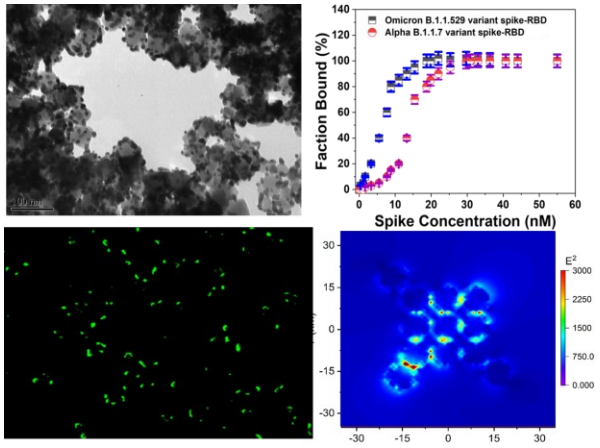


---

## 1. INTRODUCTION

Due to the emergence of mutations on the spike (S) protein gene in SARS-CoV-2 (severe acute respiratory syndrome coronavirus 2), the death toll for the COVID-19 (coronavirus disease-19) pandemic reached more than 6.2 million as of May 2022. As per Centers for Disease Control and Prevention (CDC), due to the mutations in the spike gene, different SARS-CoV-2 lineages such as B.1.1.7 (Alpha variant,), B.1.351 (Beta variant), B.1.1.28.1 (Gamma variant), B.1.617.2 (Delta variant) and B.1.1.529 (Omicron variant) have emerged. It is also reported that Omicron and Delta variants, spreads more easily than earlier variants. As it is well documented now, Omicron variant has a total of 32 mutations on the S protein, as a result, it is capable of vaccine breakthrough. Recent clinical study indicates that due to the 15 mutations in the receptor-binding domain (RBD), the delta and omicron strain has capability to escape the immune response, which has been acquired by the people in our society via COVID-19 infection or through several vaccines which are administered in last two years. All the above data clearly indicates that designing new bio-conjugated material-based strategy to separate, detect and block the omicron variant interactions are very important for our society. Driven by the need herein we report the development of magnetic-plasmonic heterostructures which synergistically exhibits magnetic and plasmonic characteristics for magnetic separation, plasmonic based SERS identification, and prevent the different variants virus entry into the host cells via blocking spike the protein RBD binding with host cells angiotensin converting enzyme 2 (ACE2).

From experimental reported data it is now well known that COVID-19 infection happens via twostep process. In the 1st step virus enter cells through the binding between the receptor binding domain (RBD) of spike protein in SARS-CoV-2 and the host receptor, angiotensin-converting enzyme 2 (ACE2) of lung cells in human body. In the 2nd step, the transmembrane protease serine 2 (TMPRSS2) helps to spread into the infected cell through endocytosis. Since the binding between spike protein RBD with ACE2 is the main pathway, we have anchored peptides derived from ACE2 with plasmonic-magnetic heterostructure for selective binding with SARS-CoV-2 variants spike RBD, as well as to block the infection.

Heterostructure composed of magnetic iron oxide and plasmonic noble metal (Au or Ag) nanoparticles, exhibits magnetic, plasmonic, and photo thermal properties have wide applications in biotechnology such as bio separation, plasmonic sensing, bioimaging, photo therapy and targeted drug delivery, etc. In our design, for the formation of magnetic-plasmonic heterostructures, we have integrated plasmonic gold nanoparticle and magnetic $Fe_2O_3$ nanoparticles together with controlled structures. Due to the presence of magnetic nanoparticle the heterostructures exhibited high superparamagnetic behavior with specific magnetization 84 emu/g Fe and it has been used for the separation of omicron variant SARS-CoV-2 viruses from biological sample using simple bar magnet. Reported experimental data shows ACE2 peptide conjugated hetero structures can be used for 100% separation of different variant of SARS-CoV-2 from infected artificial nasal mucus fluid sample. On the other hand, due to the formation of huge numbers of hot spot in the presence of SARS-CoV-2, we have achieved higher hotspot density, which allow us to achieve huge SERS enhancement for 4-aminothiolphenol (4-ATP) used as Raman reporter probe. As a result, in our design plasmonic gold nanoparticle has been used for identification of SARS-CoV-2 viruses using SERS. Similarly, ACE2 peptide in bio-conjugated hetero structure has been used to bind with spike protein RBD, as a result, no vacant spike protein RBD are available to bind with ACE2 on lung cells in human body.

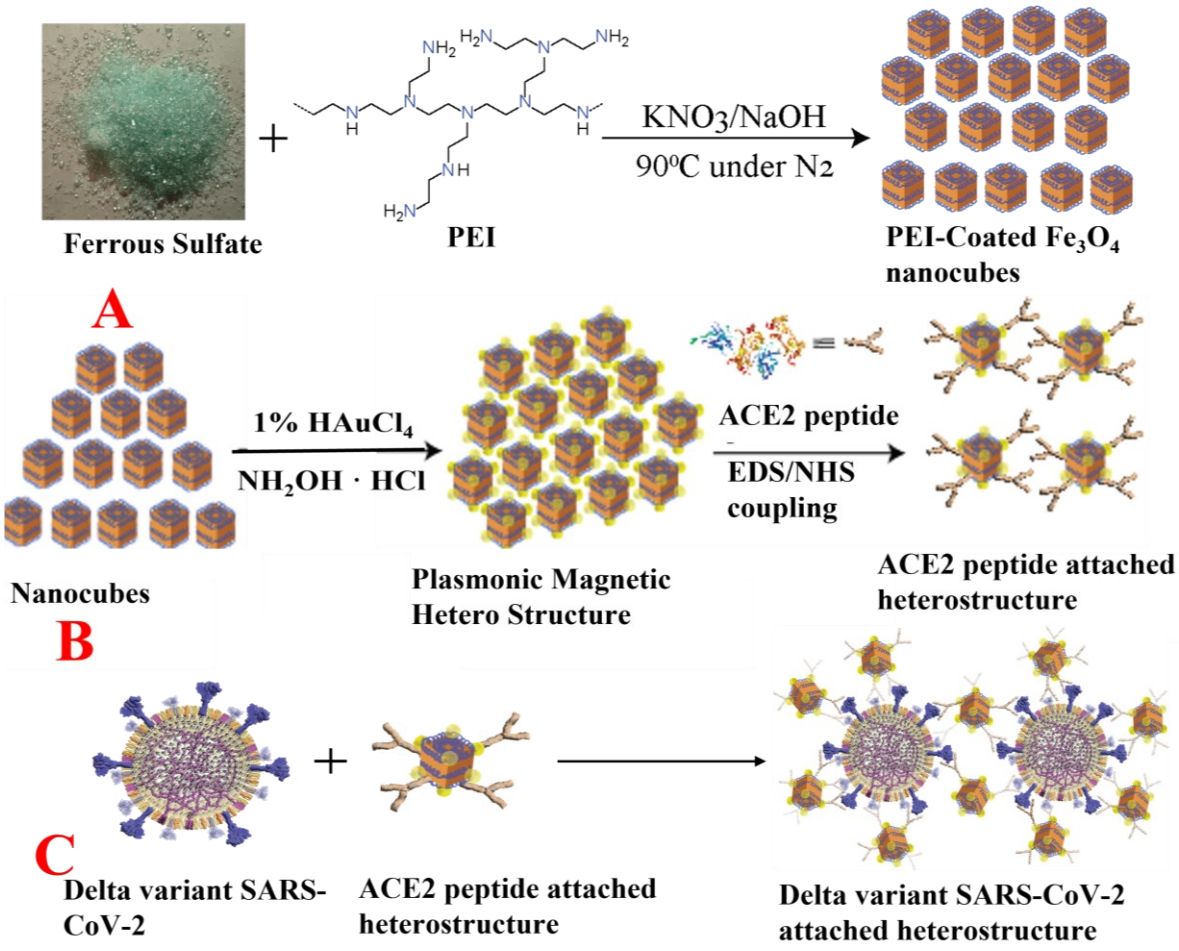


**Figure 1: A) Scheme shows synthesis path we have used for the design of PEI-coated $Fe_3O_4$ nano cubes. B) Scheme shows synthesis path we have used for the design of ACE2 peptide attached plasmonic-magnetic heterostructures. C) Scheme shows the interaction between ACE2 peptide attached heterostructure and Omicron variant SARs-CoV-2 via spike protein-ACE2 interaction.**

Reported experimental data using HEK293T-human cell line demonstrated that ACE2 peptide conjugated plasmonic-magnetic hetero structures has capability for complete inhibition of different variants SARS-CoV-2 pseudo virions entry into host cells via blocking the ACE2-spike protein RBD binding.

## 2. RESULTS and DISCUSSIONS

### 2.1 Design of ACE2 Peptide attached plasmonic-magnetic heterostructure

ACE2 Peptide attached plasmonic-magnetic heterostructure were developed in three-step process, as shown in Figure 1A-1B. In the first step, as shown in Figure 1A, PEI coated cubic shaped Fe3O4 magnetic nanoparticles were synthesized using ferrous sulfate heptahydrate, potassium nitrate, sodium hydroxide and poly ethylenimine.

Experimental details have been reported in the supporting information. In brief, the mixture was heated to 90 °C under nitrogen atmosphere with continuous stirring for 2.5 hours.

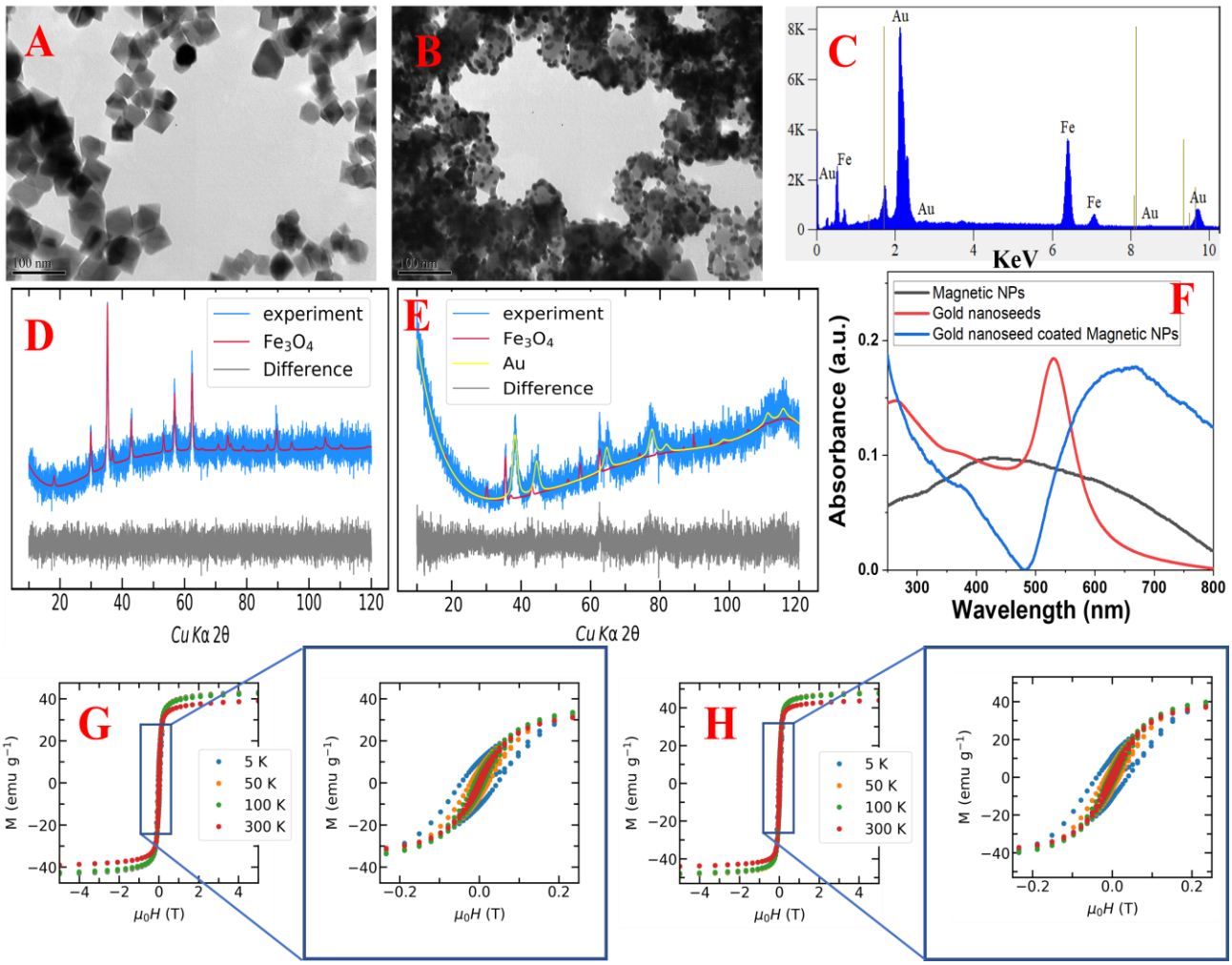


**Figure 2: A) TEM image shows the morphology of freshly prepared PEI-coated $Fe_3O_4$ nano cubes. B) TEM image shows the morphology of freshly prepared gold nanoparticle attached PEI-coated $Fe_3O_4$ nano cubes based plasmonic-magnetic heterostructures. C) Energy-dispersive X-ray spectroscopy (EDX) mapping data shows the presence of Au and Fe in plasmonic-magnetic heterostructures. D) X-ray diffraction (XRD) analysis from PEI-coated $Fe_3O_4$ nano cubes shows the presence of (012), (104), (110), (113), (202), (024), (116), (018), (214), (300), (208), (101) and (220), indices for hematite ($\alpha Fe_2O_3$) phase. E) X-ray diffraction (XRD) analysis from plasmonic-magnetic heterostructure shows the presence of (111), (200), (220), (311) and (222) indices for gold nanoparticles are face-centered cubic crystalline structure and 012), (104), (110), (113), (202), (024), (116), (018), (214), (300), (208), (101) and (220), indices for hematite ($\alpha Fe_2O_3$) phase. F) Extinction spectra from PEI-coated $Fe_3O_4$ nano cubes, gold nano seeds and gold nanoparticle attached PEI-coated $Fe_3O_4$ nano cubes based plasmonic-magnetic heterostructures. G) Temperature dependent magnetization curves for PEI-coated $Fe_3O_4$ nano cubes. H) Temperature dependent magnetization curves for gold nanoparticle attached PEI-coated $Fe_3O_4$ nano cubes based plasmonic-magnetic heterostructures.**

After that, the PEI coated cubic shaped Fe3O4 magnetic nanoparticles were separated and purified by magnetic separation and redispersion in ultrapure water for several cycles and then dried in vacuum. As shown in Figure 2A, the transmission electron microscopy (TEM) image shows the size for freshly prepared PEI-coated $Fe_3O_4$ nano cubes are 25 ± 5 nm. As shown in Table 1, the dynamic light scattering (DLS) measurement data for freshly prepared PEI-coated $Fe_3O_4$ nano cubes matches well with the TEM data reported in Table 2A. The powder X-ray diffraction (XRD) pattern from freshly prepared PEI-coated $Fe_3O_4$ nano cubes, reported in Figure 2D shows the presence of (012), (104), (110), (113), (202), (024), (116), (018), (214), (300), (208), (101) and (220) refection, which indices hematite ($\alpha Fe_2O_3$) phase. Figure 2G shows the temperature dependent magnetization curves for PEI-coated $Fe_3O_4$ nano cubes, from which we have estimated saturation magnetization to be about 34 emu/g.

In the first step, as shown in Figure 1B, initially gold nanoparticle attached PEI-coated $Fe_3O_4$ nano cubes based plasmonic-magnetic heterostructures were developed from PEI-coated $Fe_3O_4$ nano cubes using 1% $HAuCl_4$ and 2. ml of 0.2 M hydroxyl amine hydrochloride. Experimental details have been reported in the supporting information. For this purpose, gold atoms were deposited onto PEI-coated $Fe_3O_4$ nano cubes surfaces via repeated reduction of $Au^{3+}$ to $Au^0$ and nucleation of $Au^0$ by hydroxyl amine hydrochloride. In brief, PEI-coated $Fe_3O_4$ nano cubes was mechanically stirred with NaOH (pH ~12.0). After that 1 1% $HAuCl_4$ and hydroxyl amine hydrochloride were injected to the above solution where the reduced gold initiates the growth of gold seed surfaces and generates a spherical core shell of overlayered gold. Finally, gold nanoparticle attached PEI-coated $Fe_3O_4$ nano cubes based plasmonic-magnetic heterostructures were obtained by magnetitic separation followed by washed twice with water.

**Table 1**: **Size of PEI-coated $Fe_3O_4$ nano cubes, gold nanoparticle attached PEI-coated $Fe_3O_4$ nano cubes based plasmonic-magnetic heterostructures and ACE2 peptide attached heterostructure**, **measured using dynamic light scattering (DLS) and TEM techniques**

| System | DLS | TEM |
|---|---|---|
| PEI-coated $Fe_3O_4$ nano cubes | 25 ± 5 nm | 22 ± 8 nm |
| Heterostructure | 40 ± 10 nm | 40 ± 10 nm |
| ACE2 peptide attached heterostructure | 50 ± 10 nm | 40 ± 10 nm |

The solid product again resuspended in 25 ml of ultrapure water and stored at refrigerator for few months. As shown in Figure 2B, TEM image shows the size for freshly prepared gold nanoparticle attached PEI-coated $Fe_3O_4$ nano cubes based plasmonic-magnetic heterostructures are 40 ± 10 nm. As shown in Table 1, DLS measurement data for freshly prepared gold nanoparticle attached PEI-coated $Fe_3O_4$ nano cubes based plasmonic-magnetic heterostructures matches well with the TEM data reported in Figure 2. The XRD pattern from freshly prepared gold nanoparticle attached PEI-coated $Fe_3O_4$ nano cubes based plasmonic-magnetic heterostructures were, reported in Figure 2E shows the presence of (012), (104), (110), (113), (202), (024), (116), (018), (214), (300), (208), (101) and (220) indices for $Fe_2O_3$ and (111), (200), (220), (311) and (222) indices for gold. Figure 2F shows the absorption spectra for gold nanoparticle attached PEI-coated $Fe_3O_4$ nano cubes based plasmonic-magnetic heterostructures and comparison with gold nanoparticle and PEI-coated $Fe_3O_4$ nano cubes only.

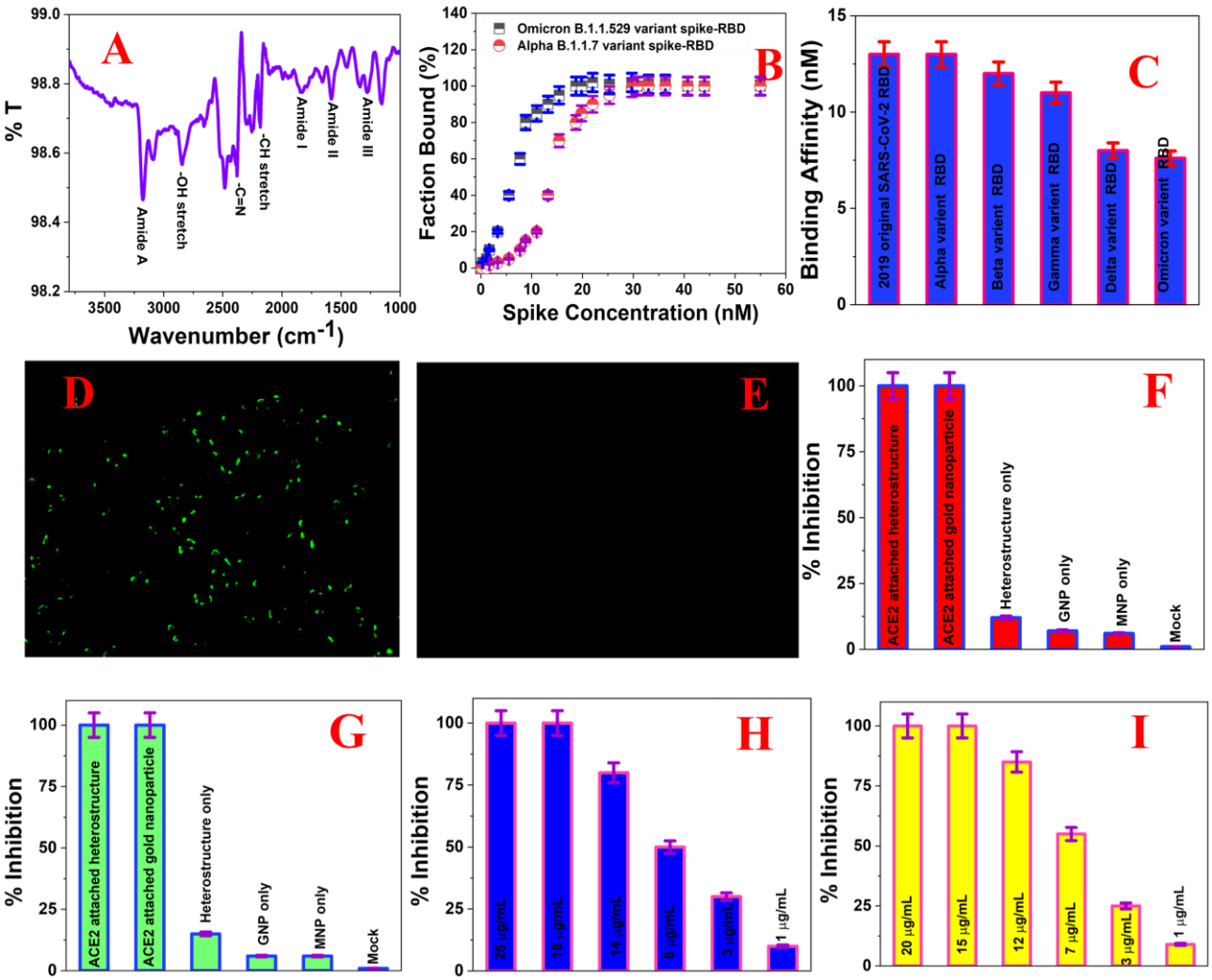


**Figure 3: A) FTIR spectra from freshly prepared ACE2 peptide attached plasmonic-magnetic heterostructures. B) Binding curve between ACE2 peptide attached plasmonic-magnetic heterostructures and Omicron variant SARS-CoV-2 spike-RBD and Alpha variant SARS-CoV-2 spike-RBD. C) Plots shows how binding affinity between ACE2 peptide attached plasmonic-magnetic heterostructures and SARS-CoV-2 spike-RBD varies for different variants. D) Inhibition of GFP tagged pseudotyped SARS-CoV-2 bearing the Delta variant spike binding to the surface of HEK-293T cells in the absence of ACE2 peptide attached plasmonic-magnetic heterostructures. Green fluorescence is due to the binding of GFP tagged pseudotyped SARS-CoV-2 bearing the Delta variant spike with HEK-293T cells expressing ACE2. E) Inhibition of pseudotyped SARS-CoV-2 bearing the Delta variant spike binding to the surface of HEK-293T cells in the presence of ACE2 peptide attached plasmonic-magnetic heterostructures. No green fluorescence is observed which indicate 100% blocking of binding. F) Inhibition efficiency of pseudotyped SARS-CoV-2 bearing the Delta variant spike in the presence of ACE2 peptide attached plasmonic-magnetic heterostructures, ACE2 peptide attached GNPs, plasmonic-magnetic heterostructures without ACE2 peptide, plasmonic GNP, magnetic nanoparticle, and buffer (Mock). G) Inhibition efficiency of pseudotyped SARS-CoV-2 bearing the original 2019 virus spike in the presence of ACE2 peptide attached plasmonic-magnetic heterostructures, ACE2 peptide attached GNPs, plasmonic-**

**magnetic heterostructures without ACE2 peptide, plasmonic GNP, magnetic nanoparticle, and buffer (Mock). H) Inhibition efficiency of pseudotyped SARS-CoV-2 bearing the Delta variant spike (10000/mL) in the presence of different amount of ACE2 peptide attached plasmonic-magnetic heterostructures. I) Inhibition efficiency of pseudotyped SARS-CoV-2 bearing the original 2019 virus spike (10000/mL) in the presence of different amount of ACE2 peptide attached plasmonic-magnetic heterostructures.**

Reported data shows the plasmonic band from heterostructures. From the reported data we have also observed very broad plasmonic band and it is due to the formation of three-dimensional (3D) hotspot by gold nanoparticles on surface of heterostructure. Figure 2H shows the temperature dependent magnetization curves for gold nanoparticle attached PEI-coated $Fe_3O_4$ nano cubes based plasmonic-magnetic heterostructures, from which we have estimated saturation magnetization to be about 40 emu/g.

Next, for the design of ACE2 peptide attached plasmonic-magnetic heterostructures, we have used carbodiimide coupling chemistry between carboxy group of peptide and amine group of PEI coated magnetic nanoparticle. For this purpose, at first, we have used 1-ethyl-3(3-(dimethylamino)-propyl) carbodiimide· HCl (EDC) and N hydroxysuccinimide (NHS) coupling agents. After stirring for 24 h, ACE2 peptide attached plasmonic-magnetic heterostructures were obtained by magnetitic separation followed by washed twice with water. Fourier-transform infrared spectroscopy (FTIR) data from ACE2 peptide attached plasmonic-magnetic heterostructures, as reported in Figure 3A shows amide A, amide-I, amide-II and amide-III bands which shows the ACE2 peptides are attached on the surface of plasmonic-magnetic heterostructures. As shown in Table 1, DLS measurement data for freshly prepared ACE2 peptide attached plasmonic-magnetic heterostructures shows the size is around 50 ± 10 nm, which is 10 nm higher than plasmonic-magnetic heterostructures without ACE2 peptides.

**2.2. Finding the Binding Affinity for different variants SARS-CoV-2 Spike Protein RBD with ACE2 Peptide attached Plasmonic-Magnetic Heterostructures**

Since the binding between the receptor binding domain (RBD) of spike protein in SARS-CoV-2 and ACE2 peptide attached plasmonic-magnetic heterostructures is the most important parameter to find out whether newly designed heterostructures has capability for blocking the COVID-19 infections, we have determined binding affinity between different variants SARS-CoV-2 RBD and ACE2 peptide attached heterostructures. For this purpose, we have used Enzyme-linked immunosorbent **(**ELISA)-like assay using His-tag protein[27-28]. Experimental details have been reported in supporting information. Initially, different variants SARS-CoV-2 RBD were adsorbed to a 96-well plate overnight at 4 °C. In next step, we have incubated blocking buffer and different amounts of ACE2 peptide attached plasmonic-magnetic heterostructures on the plate. After that streptavidin protein was used which can conjugate with horseradish peroxidase (HRP). Next, TMB (3,3',5,5'-tetramethylbenzidine) was used for colorimetric identification. At the end, the binding affinity was determined using non-linear curve fitting as we and others have reported before. Figure 3B shows the binding curve between ACE2 peptide attached plasmonic-magnetic heterostructures and Alpha variant (B.1.1.7) spike protein-RBD. The same Figure we have also reported the binding curve between ACE2 peptide attached plasmonic-magnetic heterostructures and Omicron variant (B.1.1.529) spike protein-RBD. As reported in Figure 3C, from ELISA based binding data, we have found out the binding affinity between ACE2 peptide attached plasmonic-magnetic heterostructures and spike protein-RBD of Omicron variant as 7 ± 1 nM. Similarly, are reported in Figure 3C, we have

found out the binding affinity between ACE2 peptide attached plasmonic-magnetic heterostructures and spike protein-RBD of Alpha variant as 12 ± 1 nM. Reported experimental data in Figure 3C shows the binding affinity for different variants varies as follows, Alpha < Beta < Gamma < Delta < Omicron.

### 2.3. Finding the Blocking ability of the SARS-CoV-2 original and Delta Variant (B.1.617.2) Virous infection by ACE2 Peptide attached Plasmonic-Magnetic Heterostructures using HEK-293T cells

To understand whether ACE2 peptide attached plasmonic-magnetic heterostructures have capability to prevent the COVID infection via blocking the virus entry into the host cells, we have performed blocking ability experiments using pseudotyped SARS-CoV-2 bearing the Delta variant spike as well as with pseudotyped SARS-CoV-2 bearing the original 2019 virus spike. Experimental details have been reported in the supporting information[27-28]. In brief, for both experiments we have used GFP tagged Baculovirus pseudotyped with original SARS-CoV-2 spike protein, as well as GFP tagged Baculovirus pseudotyped with SARS-CoV-2 delta variant (B.1.617.2) spike protein. For this purpose, human embryonic kidney-239T cells with a high expression of ACE2 (HEK-293T) was cultured and then incubated with ACE2 peptide attached plasmonic-magnetic heterostructures and virus.

Figure 3D shows green fluorescence image from HEK-293T cells due to the binding GFP tagged pseudotyped virus with HEK-293T cells via spike-ACE2 interaction, when ACE2 peptide attached plasmonic-magnetic heterostructures are absence. On the other hand, Figure 3E shows no fluorescence from HEK-293T cells, in the presence of ACE2 peptide attached plasmonic-magnetic heterostructures, which clearly indicate that pseudotyped virus cannot bind with HEK-293T cells. The observed no fluorescence is mainly due to the fact that, once ACE2 peptide attached plasmonic-magnetic heterostructures binds with GFP tagged pseudotyped virus spike protein, there are no empty spike protein available to bind with HEK-293T cells. Experimental observed data clearly indicates that ACE2 peptide attached plasmonic-magnetic heterostructures have capability to block Delta variant viral infection. Figure 3F shows the **i**nhibition efficiency of pseudotyped SARS-CoV-2 bearing the Delta variant spike in the presence of ACE2 peptide attached plasmonic-magnetic heterostructures, ACE2 peptide attached GNPs, plasmonic-magnetic heterostructures without ACE2 peptide, plasmonic GNP, magnetic nanoparticle and buffer (Mock). Reported data clearly shows that ACE2 peptide presence is highly impotent for 100% inhibition of virus infection. Similarly, Figure 3G shows the **i**nhibition efficiency of pseudotyped SARS-CoV-2 bearing the original 2019 virus spike in the presence of ACE2 peptide attached plasmonic-magnetic heterostructures, ACE2 peptide attached GNPs, plasmonic-magnetic heterostructures without ACE2 peptide, plasmonic GNP, magnetic nanoparticle and buffer (Mock). Reported data clearly shows that ACE2 peptide presence is highly impotent for 100% inhibition of original type SARS-CoV-2 virus infection.

Next to understand how the inhibition efficiency varies with the concentration of ACE2 peptide attached plasmonic-magnetic heterostructures. We have done **i**nhibition efficiency experiment for pseudotyped SARS-CoV-2 bearing the Delta variant spike (10,000/mL) using 1 µg/mL to 25 µg/mL, ACE2 peptide attached plasmonic-magnetic heterostructures. As reported in Figure 3H, experimental data clearly shows that 18 µg/mL ACE2 peptide attached plasmonic-magnetic heterostructures is enough for achieving 100% inhibition efficiency. Similarly, we have done **i**nhibition efficiency experiment for pseudotyped SARS-CoV-2 bearing the original 2019 virus spike (10,000/mL) using 1 µg/mL to 20 µg/mL, ACE2 peptide attached plasmonic-magnetic heterostructures.

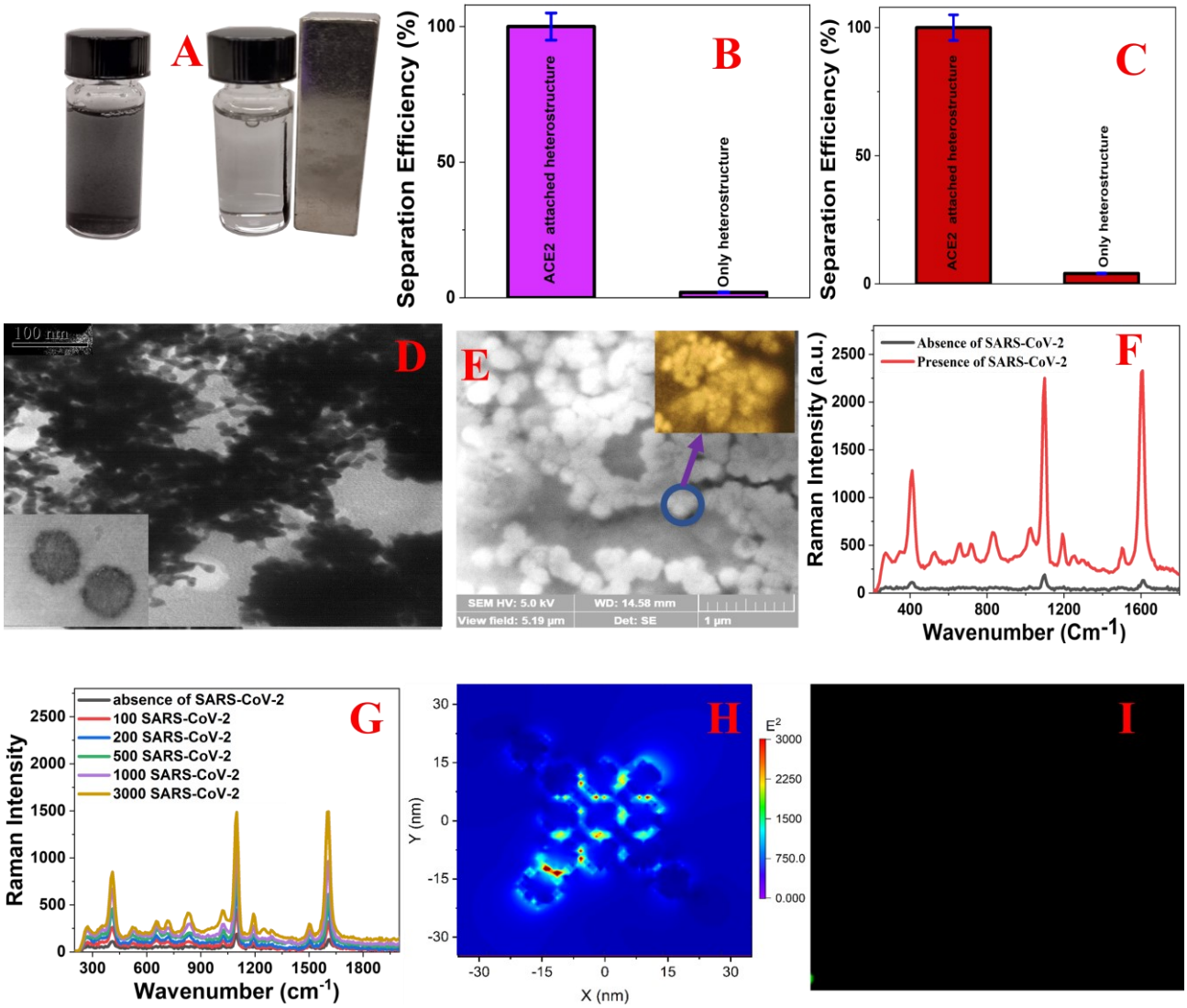


**Figure 4: A) Photograph shows effective magnetic separation of pseudotyped SARS-CoV-2 bearing the Delta variant spike from infected artificial nasal mucus fluid sample using a simple bar magnet. B) Separation efficiency for pseudotyped SARS-CoV-2 bearing the Delta variant spike from infected artificial nasal mucus fluid sample using ACE2 peptide attached plasmonic-magnetic heterostructures and plasmonic-magnetic heterostructures without ACE2 peptide. C) Separation efficiency for pseudotyped SARS-CoV-2 bearing the original 2019 virus spike from infected artificial nasal mucus fluid sample using ACE2 peptide attached plasmonic-magnetic heterostructures and plasmonic-magnetic heterostructures without ACE2 peptide. D) TEM image shows the morphology of ACE2 peptide attached plasmonic-magnetic heterostructures conjugated pseudotyped SARS-CoV-2 bearing the Delta variant spike after magnetic separation. Inserted image shows morphology of Delta variants of Pseudo SARS-CoV-2 without heterostructure. E) SEM image shows the morphology of ACE2 peptide attached plasmonic-magnetic heterostructures conjugated pseudotyped SARS-CoV-2 bearing the original 2019 virus spike, after magnetic separation. Inserted high resolution image shows the formation of "hot spot" on the surface of virus. F) SERS spectra from 4-ATP conjugated heterostructures in the absence of pseudotyped SARS-CoV-2 bearing the Delta variant spike and in the presence of pseudotyped SARS-CoV-**

**2 bearing the Delta variant spike after magnetic separation. G) SERS spectra from 4-ATP conjugated heterostructures in the presence of different amounts pseudotyped SARS-CoV-2 bearing the Delta variant spike. H) Finite-difference time-domain (FDTD) simulation data show the ($|E|^2$) profile for GNP aggregates. GNP aggregate structure has been used from SEM/TEM data. I) Inhibition of pseudotyped SARS-CoV-2 bearing the Delta variant spike binding to the surface of HEK-293T cells in the presence of ACE2 peptide attached plasmonic-magnetic heterostructures, after magnetic separation. No green fluorescence is observed which indicate 100% blocking of binding.**

As reported in Figure 3I, experimental data clearly shows that 15 µg/mL ACE2 peptide attached plasmonic-magnetic heterostructures is enough for achieving 100% inhibition efficiency.

### 2.4. Finding the Separation, identification, and inhibition ability of pseudotyped SARS-CoV-2 bearing the Delta variant spike and pseudotyped SARS-CoV-2 bearing the original 2019 virus spike from infected artificial nasal mucus fluid sample using ACE2 Peptide attached Plasmonic-Magnetic Heterostructures

To understand whether ACE2 peptide attached plasmonic-magnetic heterostructures can be used for effective magnetic separation, SERS based identification and complete inhibition of pseudotyped SARS-CoV-2 bearing the Delta variant spike from infected artificial nasal mucus fluid sample, we have performed using pseudotyped SARS-CoV-2 infected artificial nasal mucus fluid samples. For this purpose, initially we have developed 4-aminothiolphenol (4-ATP) Raman reporter attached bio-conjugated plasmonic-magnetic heterostructures. To design 4-ATP attached heterostructures, we have used Au-S conjugation chemistry to attached 4-ATP on the surface of GNPs on heterostructures. Next, for the development of infected nasal mucus samples, different concentration of pseudotyped SARS-CoV-2 bearing the Delta variant spike was added on the artificial nasal mucus (Biochemazone, Canada). After that we have added different concentration 4-ATP attached bio-conjugated plasmonic-magnetic heterostructures and kept the mixture for 30 minutes with stirring. As shown in the Figure 4A, at the end we have used a bar magnetic to separate heterostructures attached pseudotyped virus.

Figure 4D shows the TEM morphology of plasmonic-magnetic heterostructures attached pseudotyped SARS-CoV-2 bearing the Delta variant spike after magnetic separation. Next to determine the separation efficiency, we have used real time reverse transcription polymerase chain reaction (RT-PCR) technique for determining amount of Baculovirus in the artificial nasal mucus before and after the magnetic separation. As shown in Figure 4B, the separation efficiency was around 100% for pseudotyped SARS-CoV-2 bearing the Delta variant spike. Similarly, we have also performed same experiment for pseudotyped SARS-CoV-2 bearing the original 2019 virus spike. As shown in Figure 4C, the separation efficiency was around 100% for pseudotyped SARS-CoV-2 bearing the original 2019 virus spike. Figure 4E shows the SEM morphology of plasmonic-magnetic heterostructures attached pseudotyped SARS-CoV-2 bearing the original 2019 virus spike after magnetic separation. All reported experimental data clearly shows that bio-conjugated plasmonic-magnetic heterostructures have capability for 100% separation of pseudotyped SARS-CoV-2 from infected artificial nasal mucus fluid sample.

Next, we have performed SERS based identification of separated virus using 4-aminothiolphenol (4-ATP) Raman reporter attached bio-conjugated plasmonic-magnetic heterostructures. As reported in the Figure 4F, Raman intensity from 4-aminothiophenol enhanced abruptly in the pres-

ence of virus, after magnetic separation. The observed strong Raman bands at ~1590 $cm^{-1}$ can be assigned as $a_1$ vibrational modes, which is due to the $\nu$(C–C + $NH_2$ bend) vibrations. Similarly, we have also observed strong Raman bands at ~1078 $cm^{-1}$which is mainly due to $\nu$(C–C) + $\delta$(C–H)] mode. In our SERS spectra, we have also observed $b_2$ mode Raman peaks at ~1435 $cm^{-1}$ which is due to the CC stretch in Ph ring + $NH_2$ rock. Other observed strong peak at ~464 $cm^{-1}$ is due to $\nu$(C–N) + $\nu$(C–S) + $\gamma$(CCC) vibrational modes.

The observed huge enhancement of Raman intensity in the presence of pseudotyped SARS-CoV-2 bearing the Delta variant spike, is due to the formation of plasmonic-magnetic heterostructures aggregates on the surface of pseudotyped SARS-CoV-2 bearing the Delta variant spike via ACE2-spike interactions. As shown in the inserted picture in Figure 4E, heterostructures aggregates form several "hot spots", which enhances Raman signal through plasmon-excitation coupling and it is due to the strong light–matter interactions on plasmonic-magnetic heterostructures surface. To understand better on the enhancement Raman signal in the presence of pseudotyped SARS-CoV-2, we have performed Raman experiment at different concentration of virus. As shown in Figure 4G, Raman signal from 4-ATP enhanced abruptly as we increase the concentration of pseudotyped SARS-CoV-2 bearing the Delta variant spike. It is mainly due to the fact that, as we increase the number of virus, the aggregates size increases, which enhances number of "hot spot" formations. As a result, the Raman signal from 4-ATP enhanced abruptly with the concentration of pseudotyped SARS-CoV-2 .

To determine how "hot spot" formation helps to increase Raman signal, we have performed theoretical calculation using finite-difference time-domain (FDTD) simulation, as we have reported before. Details on theoretical modeling have been reported by us and others before. In brief for FDTD simulation, we have used 10 nm spherical gold nanoparticles, as we have observed in the TEM image, reported in Figure 2B. For our FDTD simulation**,** GNP aggregate structure has been used from TEM/SEM data, as reported in Figure 3D and 3E. In our FDTD simulation, we have used 670 nm wavelength, 0.001 nm mesh resolution, and 4000 fs time, as we have reported before. As reported in Figure 4H, the square of field ($|E|^2$) enhances 3000 times in "hot spots". As we and others have reported before, Raman enhancement is proportional to $|E|^4$, as a result, from FDTD simulation data shows 6 orders of magnitude Raman enhancement due to the "hot spot" formations.

Next, we have determined infection ability for plasmonic-magnetic heterostructures attached pseudotyped SARS-CoV-2 bearing the Delta variant spike, after magnetic separation. For this purpose, human embryonic kidney-239T cells with a high expression of ACE2 (HEK-293T) was cultured and then incubated with plasmonic-magnetic heterostructures attached GFP tagged pseudotyped SARS-CoV-2 bearing the Delta variant spike after magnetic separation. Figure 4I shows no fluorescence from HEK-293T cells, which clearly indicate that plasmonic-magnetic heterostructures attached pseudotyped SARS-CoV-2 cannot bind with HEK-293T cells. The observed no fluorescence is mainly due to the fact that, once ACE2 peptide attached plasmonic-magnetic heterostructures binds with pseudotyped SARS-CoV-2 virus spike protein, there are no empty spike protein available to bind with HEK-293T cells. Reported experimental data clearly shows that plasmonic-magnetic heterostructures attached pseudotyped SARS-CoV-2 bearing the Delta variant spike has no infection ability.

## 4. CONCLUSION

In conclusion, in this article we have demonstrated that ACE2 peptide attached plasmonic-magnetic heterostructures can be used for effec-

tive magnetic separation of pseudotyped SARS-CoV-2 bearing the Delta variant spike from infected artificial nasal mucus fluid sample using a simple bar magnet. Our reported binding data between ACE2 conjugated plasmonic-magnetic heterostructure and spike- receptor-binding domain (RBD) of different SARS-CoV-2 lineages such as B.1.1.7 (Alpha variant,), B.1.351 (Beta variant), B.1.1.28.1 (Gamma variant), B.1.617.2 (Delta variant) and B.1.1.529 (Omicron variant) indicates omicron has maximum binding ability and it follows Alpha < Beta < Gamma < Delta < Omicron. Reported SERS data shows due to the formation of huge "hot spots" in the presence of SARS-CoV-2, 4-ATP Raman reporter-based Raman intensity can be sued for the identification of separated virus. Theoretical FDTD simulation reported here indicates due to the "hot spots" formation six orders of magnitude Raman enhancement can be observed. Using HEK293T-human cell line and pseudotyped SARS-CoV-2 bearing the Delta variant spike as well as pseudotyped SARS-CoV-2 bearing original 2019 virus spike, we have shown that plasmonic-magnetic heterostructures attached pseudotyped SARS-CoV-2 has no infection ability. Experimental concentration dependent inhibition efficiency investigation indicates that ACE2 peptide conjugated plasmonic-magnetic hetero structures has capability for complete inhibition of Delta variants and original SARS-CoV-2 pseudo virions entry into host cells.

## 5. ACKNOWLEDGEMENTS

Dr. Ray thanks NSF-RAPID grant # DMR-2030439 and NSF-PREM grant # DMR-1826886 for their generous funding. We also thank NIH-NIMHD grant # 1U54MD015929-01for bioimaging core facility. Dr. Tandon is supported by NASA award (80NSSC19K1603) and COVID-19 funds from the University of Mississippi Medical Center.

**6. SUPORTING INFORMATIONS**: Design and characterization of the ACE2 peptide attached plasmonic-magnetic heterostructures and other experiments such as binding affinity measurement, virus inhibition experiments are available as supporting information. This information is available free of charge via the Internet at http://pubs.acs.org/.

## 7. REFERENCES

1. Altmann, D. M.; Boyton, R. J.; Beale, R. Immunity to Sars-Cov-2 Variants of Concern. *Science* **2021**, *371*, 1103– 1104.
2. Gupta, R. K. Will SARS-CoV-2 Varients of Concern Affect the Promise of Vaccines?. *Nat. Rev. Immunol.* **2021**, *21*, 340– 341.
3. Han, Y.; Yang, Z.; Hu, H.; Zhang, H.; Chen, L.; Li, K.; Kong, L.; Wang, Q.; Liu, B.; Wang, M.; Lin, J. ; Chen, P. R.; Covalently Engineered Protein Minibinders with Enhanced Neutralization Efficacy against Escaping SARS-CoV-2 Variants, *J. Am. Chem. Soc.* **2022**, 144, 13, 5702–5707
4. V'kovski, P.; Kratzel, A.; Steiner, S.; Stalder, H.; Thiel, V. Coronavirus biology and replication: implications for SARS-CoV-2. *Nat. Rev. Microbiol.* **2021**, *19*, 155– 170.
5. Mathieu, E.; Ritchie, H.; Ortiz-Ospina, E.; Roser, M.; Hasell, J.; Appel, C.; Giattino, C.; Rodés-Guirao, L. A Global Database of COVID-19 Vaccinations. *Nat. Hum. Behav.* **2021**, *5*, 947– 953
6. Müller K, Girl P, Giebl A, von Buttlar H, Dobler G, Bugert JJ, Gruetzner S, Wölfel R Emerging SARS-CoV-2 variant B.1.1.7 reduces neutralisation activity of antibodies against wildtype SARS-CoV-2. *J Clin Virol* **2021**, 142, 104912.
7. Wang, P.; Nair, M. S.; Liu, L.; Iketani, S.; Luo, Y.; Guo, Y.; Wang, M.; Yu, J.; Zhang, B.; Kwong, P. D.; Graham, B. S.; Mascola, J. R.; Chang, J. Y.; Yin, M. T.; Sobieszczyk, M.; Kyratsous, C. A.; Shapiro, L.; Sheng, Z.; Huang, Y.; Ho, D. D. Antibody resistance of SARS-CoV-2 variants B. 1.351 and B. 1.1. 7. *Nature* **2021**, *593*, 130– 135
8. Starr, T. N.; Greaney, A. J.; Addetia, A.; Hannon, W. W.; Choudhary, M. C.; Dingens, A. S.; Li, J. Z.; Bloom, J. D. Prospective Mapping of Viral

Mutations That Escape Antibodies Used to Treat Covid-19. *Science* **2021**, *371*, 850

9. Chen, J.; Gao, K.; Wang, R.; Wei, G.-W. Prediction and mitigation of mutation threats to COVID-19 vaccines and antibody therapies. *Chemical Science* **2021**, *12*, 6929–6948
10. Fontanet, A.; Autran, B.; Lina, B.; Kieny, M. P.; Karim, S. S. A.; Sridhar, D. SARS-CoV-2 variants and ending the COVID-19 pandemic. *Lancet* **2021**, *397*, 952– 954
11. Pomplun, S.De Novo Discovery of High-Affinity Peptide Binders for the SARS-CoV-2 Spike Protein. *ACS Cent. Sci.* **2021**, *7*, 156– 163
12. hen, J.; Wang, R.; Gilby, N. B.; Wei, G.-W. Omicron Variant (B. 1.1. 529): Infectivity, Vaccine Breakthrough, and Antibody Resistance. *J. Chem. Inf. Model.* **2022**,
13. Pomplun, S.De Novo Discovery of High-Affinity Peptide Binders for the SARS-CoV-2 Spike Protein. *ACS Cent. Sci.* **2021**, *7*, 156– 163
14. Pramanik, A., Gao, Y., Patibandla, S., Gates, K., and Ray, P. C. Bioconjugated Nanomaterial for Targeted Diagnosis of SARS-CoV-2. *Acc. Mater. Res.* **2022**, 3, 2, 134–148
15. Pramanik, A., Sharma, P. C.; Patibandla, Gao, Y., Ruppa-Kasani, V.; Goli, J.; Kumar, A.; Chatterjee, A.; Sinha, S. S.; Bates, J. T.; Bierdeman, M. A.; Tandon, R., and Ray, P. C. Blocking SARS-CoV-2 Delta Variant (B.1.617.2) Spike Protein Receptor-Binding Domain Binding with the ACE2 Receptor of the Host Cell and Inhibiting Virus Infections Using Human Host Defense Peptide-Conjugated Graphene Quantum Dots. *ACS Omega* **2022**, 7, 9, 8150–8157
16. Jang, A. S.; Prabhakaran, P.; Kumar, P.; Lim, K. D.; Attomolar Sensitive Magnetic Microparticles and a Surface-Enhanced Raman Scattering-Based Assay for Detecting SARS-CoV-2 Nucleic Acid Targets, *ACS Appl. Mater. Interfaces* **2022**, 14, 1, 138–149
17. Kevadiya, B. D.; Machhi, J.; Herskovitz, J.; Oleynikov, M. D.; Blomberg, W. R.; Bajwa, N.; Soni, D.; Das, S.; Hasan, M.; Patel, M.; Senan, A. M.; Gorantla, S.; Mcmillan, J.; Edagwa, B.; Eisenberg, R.; Gurumurthy, C. B.; Reid, S. P. M.; Punyadeera, C.; Chang, L.; Gendelman, H. E. Diagnostics for SARS-CoV-2 Infections. *Nat. Mater.* **2021**, *20*, 593–605
18. Ai, X.; Wang, D.; Honko, A.; Duan, Y.; Gavrish, I.; Fangh, R. H.; Griffiths, A.; Gao, W.; Zhnag, L.; Surface Glycan Modification of Cellular Nanosponges to Promote SARS-CoV-2 Inhibition, *J. Am. Chem. Soc.* **2021**, 143, 42, 17615–17621
19. Pramanik, A., Gao, Y., Patibandla, S., Mitra, D., McCandless, M. G., Fassero, L. A., Gates, K., Tandon, R., and Ray, P. C. Aptamer conjugated gold nanostar-based distance-dependent nanoparticle surface energy transfer spectroscopy for ultrasensitive detection and inactivation of corona virus. *J. Phys. Chem. Lett*. **2021**, 12, 2166–2171
20. Zhong, J.; Rösch, E. L.; Viereck, T.; Schilling, M.; Ludwig, F. Toward rapid and sensitive detection of SARS-CoV-2 with functionalized magnetic nanoparticles. *ACS Sens.* **2021**, *6*, 976– 984
21. Pramanik, A., Gao, Y., Patibandla, S., Mitra, D., McCandless, M. G., Fassero, L. A., Gates, K., Tandon, R., and Chandra Ray, P. The rapid diagnosis and effective inhibition of coronavirus using spike antibody attached gold nanoparticles. *Nanoscale Adv*. **2021**, 3, 1588–1596
22. Wang C, Wang S, Li D, Chen P, Han S, Zhao G, Chen Y, Zhao J, Xiong J, Qiu J, Wei DQ, Zhao J, Wang J. Human Cathelicidin Inhibits SARS-CoV-2 Infection: Killing Two Birds with One Stone, *ACS Infect Dis*. **2021** 11, 7,1545-1554
23. Mahmud, N.: Anik, M. I.; Hossain, M. K.; Khan, M. I.; Uddin, S.; Ashrafuzzaman, Md.; Rahaman. M. M.; Advances in Nanomaterial-Based Platforms to Combat COVID-19: Diagnostics, Preventions, Therapeutics, and Vaccine Developments. *ACS Applied Bio Materials* **2022**, Article ASAP.
24. Huergo L. F.; Selim K. A.; Conzentino M. S.; Gerhardt E. C. M.; Santos A. R. S.; Wagner B.; Alford J. T.; Deobald N.; Pedrosa F. O.; De Souza E. M.; Nogueira M. B.; Raboni S. M.; Souto D.; Rego F. G. M.; Zanette D. L.; Aoki

M. N.; Nardin J. M.; Fornazari B.; Morales H. M. P.; Borges V. A.; Nelde A.; Walz J. S.; Becker M.; Schneiderhan-Marra N.; Rothbauer U.; Reis R. A.; Forchhammer K. Magnetic Bead-Based Immunoassay Allows Rapid, Inexpensive, and Quantitative Detection of Human SARS-CoV-2 Antibodies. *ACS Sens.* 2021, 6, 703–708

25. Wang, T.: Fang, X.: Wen, T.: Liu, J.: Zhai, Z.: Wang, Z.: Meng, J.: Yang, Y.: Wang, C.: Xu, H.: Synthetic Neutralizing Peptides Inhibit the Host Cell Binding of Spike Protein and Block Infection of SARS-CoV-2, *J. Med. Chem.* **2021**, 64, 19, 14887–14894
26. Xi, H.: Jiang, H.; Juhas, M.; Zhang, Y.; Multiplex Biosensing for Simultaneous Detection of Mutations in SARS-CoV-2, *ACS Omega* 2021, 6, 40, 25846–25859
27. Kang, Y.-F.; Sun, C.; Zhuang, Z.; Yuan, R.-Y.; Zheng, Q.; Li, J.-P.; Zhou, P.-P.; Chen, X.-C.; Liu, Z.; Zhang, X.Rapid development of SARS-CoV-2 spike protein receptor-binding domain self-assembled nanoparticle vaccine candidates. *ACS Nano* **2021**, *15*, 2738– 2752
28. Larue, R. C.; Xing, E.; Kenney, A. D.; Zhang, Y.; Tuazon, J. A.; Li, J.; Yount, J. S.; Li, P. K.; Sharma, A. Rationally Designed ACE2-Derived Peptides Inhibit SARS-CoV-2. *Bioconjugate Chem.* **2021**, *32*, 215– 223
29. Tandon R, Mitra D, Sharma P, McCandless MG, Stray SJ, Bates JT, Marshall GD. Effective screening of SARS-CoV-2 neutralizing antibodies in patient serum using lentivirus particles pseudotyped with SARS-CoV-2 spike glycoprotein. *Sci Rep*. **2020,** 5, 10(1), 19076.
30. Tandon R, Sharp JS, Zhang F, Pomin VH, Ashpole NM, Mitra D, McCandless MG, Jin W, Liu H, Sharma P, Linhardt RJ. Effective Inhibition of SARS-CoV-2 Entry by Heparin and Enoxaparin Derivatives. *J Virol*. **2020**, 95, e01987-20
31. Pramanik, A., Vangara, A., Nellore, B. B. P. V., Sinha, S. S., Chavva, S, R., Jones, S., Ray, P. C. Development of Multifunctional Fluorescent−Magnetic Nanoprobes for Selective Capturing and Multicolor Imaging of Heterogeneous Circulating Tumor Cells. *ACS Appl. Mater. Interfaces.* **2016**, *8*, 15076–15085.
32. Ian Y. Goon, Lai, L. M. H., Lim, M., Munroe, P., Gooding, J. J., Amal, R. Fabrication and Dispersion of Gold-Shell-Protected Magnetite Nanoparticles: Systematic Control Using Polyethyleneimine. *Chem. Mater.* **2009**, *21*, 673–681.
33. Felix, L. L.; Sanz, B.; Sebastian, V.; Torres, T. E.; Sousa, M. H.; Coaquira, J. H.; Ibarra, M. R.; Goya, G. F.; Gold-decorated magnetic nanoparticles design for hyperthermia applications and as a potential platform for their surface-functionalization, *Sci. Rep*. **2019**, 9, 4185.
34. Sinha, S. S.; Jones, S.; Pramanik, A.; Ray, P. C. Nanoarchitecture Based SERS for Biomolecular Fingerprinting and Label-Free Disease Markers Diagnosis. *Acc. Chem. Res.* **2016**, *49*, 2725– 2735
35. Matricardi, C.; Hanske, C.; Garcia-Pomar, J. L.; Langer, J.; Mihi, A.; Liz-Marzán, L. M. Gold Nanoparticle Plasmonic Superlattices as Surface-Enhanced Raman Spectroscopy Substrates. *ACS Nano* **2018**, *12*, 8531– 8539
36. Pramanik, A.; Mayer, J.; Patibandla, S.; Gates, K.; Gao, Ye; Davis, D.; Seshadri, R.; Ray, P. C. Mixed-Dimensional Heterostructure Material-Based SERS for Trace Level Identification of Breast Cancer-Derived Exosomes. *ACS-Omega* **2020**, *5* (27), 16602– 16611
37. Gong, L.; Zheng, W.; Ma, Y.; Huang, Z. Higher-order coherent anti-Stokes Raman scattering microscopy realizes label-free super-resolution vibrational imaging. *Nat. Photonics* **2020**, *14*, 115– 122
38. Langer, J.; Jimenez de Aberasturi, D.; Aizpurua, J.; Alvarez-Puebla, R. A.; Auguié, B.; Baumberg, J. J.; Bazan, G. C.; Bell, S. E.; Boisen, A.; Brolo, A. G.*et al.*Present and future of surface-enhanced Raman scattering. *ACS Nano* **2020**, *14*, 28– 117